At-wavelength interferometry for extreme ultraviolet lithography

Edita Tejnil,[a] Kenneth A. Goldberg,[b] SangHun Lee,[a] Hector Medecki, Phillip J. Batson, and Paul E. Denham
Center for X-Ray Optics, Lawrence Berkeley National Laboratory, Berkeley, California 94720

Alastair A. MacDowell
Advanced Light Source, Lawrence Berkeley National Laboratory, Berkeley, California 94720

Jeffrey Bokor[a),c)] and David Attwood[a)]
Center for X-Ray Optics, Lawrence Berkeley National Laboratory, Berkeley, California 94720

(Received 27 May 1997; accepted 9 July 1997)

A phase-shifting point diffraction interferometer is being developed for at-wavelength testing of extreme ultraviolet lithographic optical systems. The interferometer was implemented to characterize the aberrations of a 10× Schwarzschild multilayer-coated reflective optical system at the operational wavelength of 13.4 nm. Chromatic vignetting effects are observed and they demonstrate the influence of multilayer coatings on the wave front. A subaperture of the optic with a numerical aperture of 0.07 was measured as having a wave front error of 0.090 wave (1.21 nm) root mean square (rms) at a 13.4 nm wavelength. The wave front measurements indicate measurement repeatability of ±0.008 wave (±0.11 nm) rms. Image calculations that include the effects of the measured aberrations are consistent with imaging performed with the 10× Schwarzschild optic on an extreme ultraviolet exposure tool. © *1997 American Vacuum Society.* [S0734-211X(97)01306-1]

I. INTRODUCTION

Wave front measuring interferometry plays a key role in the fabrication, alignment, and qualification of optical systems, including lithographic stepper lenses. Interferometric characterization of extreme ultraviolet (EUV) projection lithography optics is necessary to achieve the near diffraction-limited optical performance required for lithography at critical dimensions of 0.1 μm and below. Such EUV lithographic optical systems operate at a wavelength of about 13 nm with numerical apertures of around 0.1. To characterize the aberrations, interferometry with subnanometer wave front measuring accuracy is required. In addition, measurements at an operational wavelength of 13 nm are needed to characterize the system EUV wave front, which is produced both by the figure of mirror surfaces and by multilayer coating properties.[1] Common-path techniques, such as point diffraction interferometry[2] or shearing interferometry,[3] are required for at-wavelength wave front characterization due to the lack of long-coherence-length light sources at EUV wavelengths.

Point diffraction interferometry is suitable for direct measurement of wave front aberrations at EUV wavelengths because of its applicability over a wide spectral range, compact design, and relaxed temporal coherence length requirements.[2] This technique utilizes the generation of a high-quality spherical reference wave front by diffraction from a ''subresolution'' pinhole. This reference wave front interferes with the unknown wave front under test. We have recently developed a phase-shifting point diffraction interferometer (PS/PDI) that enables EUV wave front characterization with both high efficiency and a phase-shifting capability.[4–6]

In this article, we describe recent measurements of a 10× demagnification, multilayer-coated, Schwarzschild objective, designed for a prototype EUV lithography exposure tool[7] using the new phase-shifting point diffraction interferometer. The repeatability of the interferometric measurements is characterized. The aberrations of the optical system are described, and a demonstration of chromatic aberrations due to multilayer coatings is also presented. Finally, the optical performance predicted by the interferometry is verified by imaging experiments utilizing the EUV exposure tool for which the optic was designed.

II. INTERFEROMETER CONFIGURATION FOR TESTING THE 10× SCHWARZSCHILD SYSTEM

The phase-shifting point diffraction interferometer for at-wavelength testing of EUV lithographic optics operates at the undulator beamline 12.0 at the Advanced Light Source (ALS) at Lawrence Berkeley National Laboratory. The beamline optics include a grating monochromator that is used to select the desired wavelength, and a Kirkpatrick–Baez (KB) illuminator that is designed for optimum transfer of spatially coherent radiation to the interferometer.

The Schwarzschild test optic, designed for 10× reduction EUV projection lithography experiments, consists of two nearly concentric spherical mirrors.[7] Both mirrors are coated with molybdenum–silicon multilayer reflective coatings with peak transmission at 13.4 nm wavelength. While the annular, concave secondary is coated with a multilayer of nearlly uniform thickness, the convex primary has a graded multilayer coating designed to compensate for the varying angles of

[a)]Also at Dept. of Electrical Engineering and Computer Sciences, University of California, Berkeley, CA 94720.
[b)]Also at Dept. of Physics, University of California, Berkeley, CA 94720.
[c)]Electronic mail: jbokor@eecs.berkeley.edu

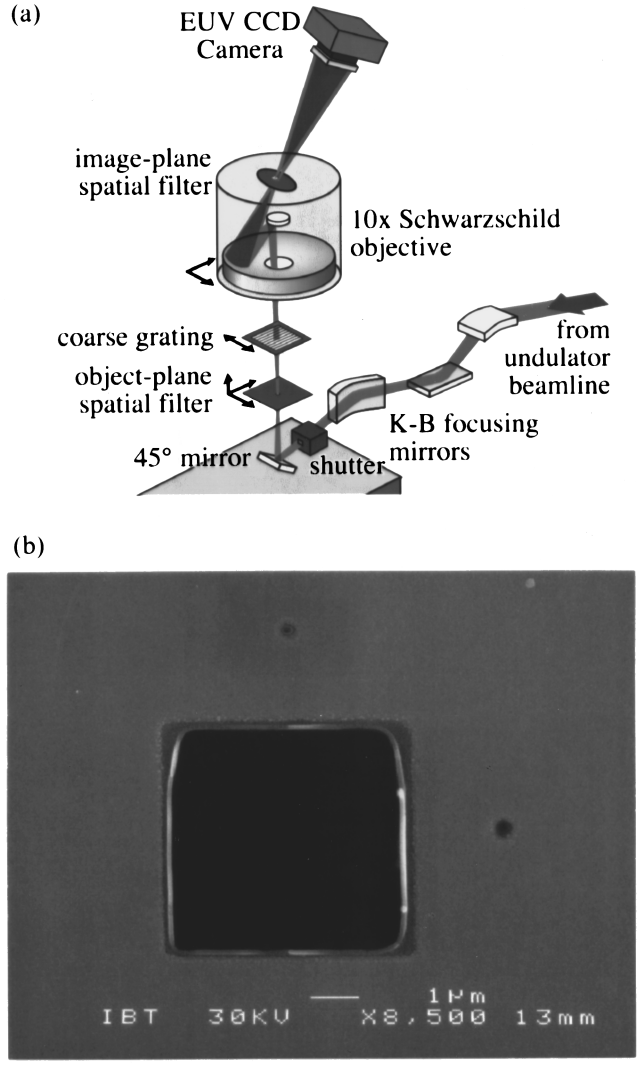

FIG. 1. (a) Components of the phase-shifting point diffraction interferometer for testing the 10× demagnification Schwarzschild optical system. (b) A SEM image of the spatial filter used in the image plane of the Schwarzschild optic. Two subresolution pinholes with diameters of 130 nm (top) and 165 nm (right) are next to a 5-μm×5-μm sq window.

incidence across its surface.[8] An off-axis aperture stop that rests on the primary mirror can select a circular portion of the annular clear aperture for imaging experiments. This rotatable aperture stop contains three separate subapertures, corresponding to different selectable numerical apertures (NA) of 0.06, 0.07, and 0.08. The image plane of the optic, determined during the assembly of the system, is defined by three balls attached to the optical housing.

The configuration of the phase-shifting point diffraction interferometer for testing the 10× Schwarzschild optical system is illustrated in Fig. 1(a). The optic is tested in its intended vertical operational orientation. The EUV beam is steered into the optic with an adjustable, multilayer-coated, 45° turning mirror. This mirror enables small angular adjustments in the beam direction that are needed to optimize the illumination of the optic. The KB optics focus the beam onto the object plane of the 10× Schwarzschild system, where a subresolution pinhole is placed. The pinhole selects spatially coherent radiation from the beam and spatially filters it to illuminate the test optic with a spherical wave front. The object–plane pinholes used in these measurements are commercially available, laser-drilled pinholes with nominal diameters of 0.5 μm. These pinholes are significantly smaller than the diffraction-limited resolution of the test optic on the object side (subresolution), ensuring a high-quality illumination wave front.[9] This pinhole is placed in a kinematic mount attached to a computer-controlled, three-axis stage that allows alignment of the pinhole within the beam.

A coarse diffraction grating, placed between the object–plane pinhole and the Schwarzschild optic, serves as a low-angle beamsplitter by dividing the wave front into multiple diffractive orders. The 18-μm-pitch grating consists of a 225-nm-thick patterned gold absorber supported by a 100-nm-thick silicon nitride membrane. On propagation through the test optic, the aberrations of interest are introduced into the spherical illumination beams. Two of the diffractive orders are selected with a spatial filter, shown in Fig. 1(b), placed in the image plane of the optic. The zero diffractive order is chosen as the test beam and is transmitted through the large 5-μm×5-μm sq window, which is significantly larger than the focal spot size. One of the first diffractive orders is spatially filtered by a subresolution pinhole to produce a spherical reference wave front over the numerical aperture of the measurement. The choice of the zero diffractive order for the test beam ensures that aberrations due to the grating line placement are not introduced into the measured wave front. Translation of the grating in the direction perpendicular to its lines controls the relative phase shift between the test and reference beams necessary to perform phase-shifting interferometry. The grating pitch is chosen to provide a 4.5 μm separation between the test and the reference wave foci in the image plane. This corresponds to the distance between the subresolution pinhole and the center of the window. Two separate reference pinholes, placed in two orthogonal directions from the center of the test-beam window, allow measurement with two different grating orientations.

The image–plane pinhole apertures were drilled by a focused ion beam into a membrane structure consisting of 100 nm of silicon nitride and 100 nm of indium antimonide absorber. After the aperture definition, an additional 70 nm layer of indium antimonide absorber was deposited on each side of the membrane to increase the absorption and also to decrease the pinhole size. The pinholes fabricated with this method and used in experiments reported here range from 130 to 165 nm in diameter. The pinholes are aligned and fixed to be at the center of the image plane by means of a kinematic mount that rests on the three balls that define the image plane.

The interference of the test and reference beams is recorded with a back-thinned, back-illuminated, 1024×1024-pixel, 1-in. sq, silicon charge coupled device (CCD) detector, placed 12.7 cm beyond the image plane of the Schwarzschild optic with its surface normal to the central

ray of the off-axis beam. The exposure time, typically 5–15 s, is controlled with a compact, high-speed shutter placed in front of the 45° turning mirror, as shown in Fig. 1(a).

In its EUV configuration, the PS/PDI records the interference between test and reference beams without reimaging optics. To prevent beam overlap in the image plane, the lateral separation of the two beam foci is designed to be quite large. As a result, in addition to the aberrations of interest, the recorded interference fringes contain a large tilt in the direction of the beam separation. The geometrical effect of the beam separation also produces various orders of coma in the fringe pattern. For the beam separations and numerical apertures used in this experiment, only the third order coma is relevant. This systematic effect can be removed from the measured aberrations because its orientation is known to be perpendicular to the tilt fringes and its magnitude scales with the measurement numerical aperture in a known way. Combining the measurements performed with two orthogonal grating orientations makes removal of this coma effect straightforward.

Alignment of the test and reference beams through the system is accomplished by high-precision translation of the optic and the attached pinhole apertures on a bearing in two lateral directions. The focus is controlled by translation of the object–plane pinhole along the beam propagation direction. When aligned for data acquisition, the interferometer remains in alignment for several hours, and it has demonstrated good mechanical stability despite the fact that the temperature of the system is not controlled. Measured vacuum chamber temperature fluctuations typically do not exceed $\pm 0.5\,^{\circ}\mathrm{C}$ over 24 h.

To mitigate the carbon contamination problem reported recently,[6] several improvements have been made to the interferometer vacuum system, including the cleaning of most of the interferometer components and increasing the pumping speed to achieve a base pressure of 5×10^{-7} Torr. In operation during exposure to EUV light, oxygen gas is bled into the chamber to reduce carbon contamination buildup, maintaining a pressure of 10^{-4} Torr. These measures have nearly eliminated the contamination problem.

III. RESULTS OF INTERFEROMETRIC MEASUREMENTS

Numerous experiments have been done to characterize the aberrations in the Schwarzschild optic and to evaluate the capabilities of the interferometer. The measurements include characterization of several regions of the annular full aperture, evaluation of aberrations at different wavelengths, and determination of measurement repeatability.

One important measurement is to characterize the light transmitted through the uniformly illuminated test optic. The transmitted intensity of 13.4 nm radiation is shown in Fig. 2(a), which reveals localized contamination of the optical surfaces. Some of the contaminants, most likely particulates on the mirror surfaces, cause complete loss of transmission. Other contaminants, possibly a residue from a wet-cleaning process of the optical substrates or the coated surfaces, lead to reduction in the transmitted intensity. The contaminated regions are on the order of 100 μm in size. When the measurement is repeated at a visible wavelength of 632.8 nm, shown in Fig. 2(b), the transmitted intensity is quite different. The particulate contamination produces a loss of transmission, but the other residue is nearly imperceptible. Overall, the contamination effects are more pronounced at EUV wavelengths than at visible wavelengths. Mirror surface contamination present in this Schwarzschild optic scatters radiation to moderate angles and contributes to wave front aberrations in the midspatial-frequency regime. In PS/PDI measurements, some of the scatter in the reference beam is transmitted through the test-beam window. Although this corrupts the measurement in the vicinity of the contaminated regions in the aperture, it does not affect the ability of the interferometer to measure low-order aberrations.

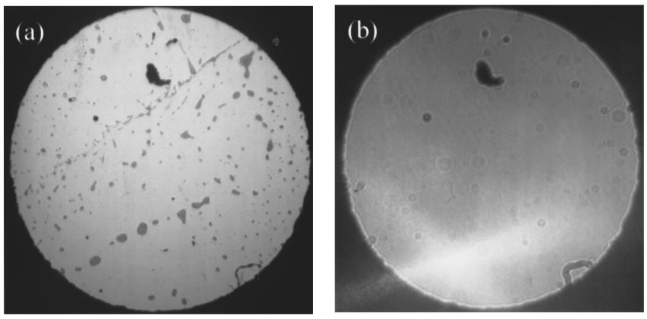

FIG. 2. Transmission of light through the Schwarzschild optic at two different wavelengths: (a) 13.4 and (b) 632.8 nm. The contamination of the optical surfaces appears quite different at the two wavelengths.

The measurements reported here utilize phase-shifting interferometry techniques that combine multiple interferograms with different relative phase shifts between the test and reference beams. Analysis of individual phase-shifting data series is performed using an adaptive least-squares algorithm,[10] modified to compensate for irregular phase increments caused by a coarsely controlled grating translation stage. The presence of numerous blemishes on the optic complicates both the phase unwrapping and the Zernike polynomial fitting. The unwrapping of the raw phase maps uses a highly filtered, continuous version of the phase maps as a guide to determine the correct phase increments.[11] The unwrapped phase maps are fitted to the first 37 Zernike circular polynomials[12] that describe the low-spatial-frequency aberrations of interest. Fitting utilizes an intermediate set of polynomials, orthogonal over the domain of valid data points that excludes the blemish regions.[13,14] Following the Zernike fit, the geometrical coma effect is removed by combining separate measurements performed with two orthogonal grating orientations.

Three different regions of the annular aperture of the $10\times$ Schwarzschild optic, corresponding to the three subapertures in the aperture stop, were characterized at 13.4 nm wavelength. The wave front aberrations of the three subapertures, reconstructed from the Zernike polynomial fit, are shown in Fig. 3. Figure 3(a) shows the relative positions of the different subapertures in the aperture stop. The largest

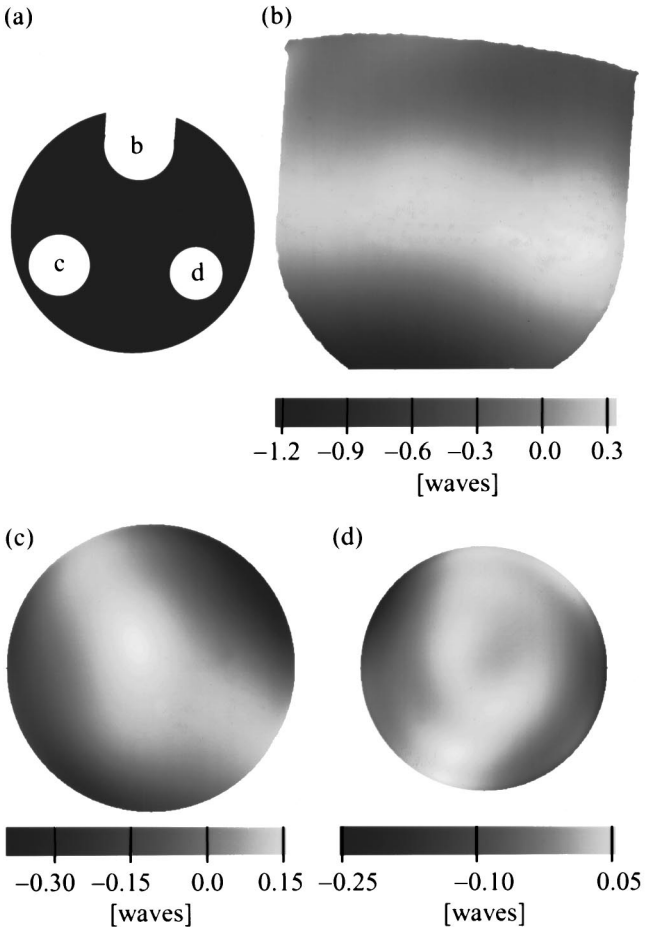

FIG. 3. Optical path difference measured in three different portions of the annular clear aperture at 13.4 nm wavelength. Each aberration profile (b)–(d) corresponds to a different subaperture on the aperture stop (a).

subaperture is noncircular due to a fabrication error. The aberrations of the 0.08, 0.07, and 0.06 NA subapertures are shown in Figs. 3(b)–3(d), respectively. Visible-light interferometry, performed during assembly of the optic, was used to align the least aberrated region of the optic with the 0.07 NA subaperture. With the tilt and defocus removed, the measured wave front errors of the 0.08, 0.07, and 0.06 NA subapertures are, respectively, 0.260, 0.090, and 0.043 wave root mean square (rms) at 13.4 nm. Figure 3 shows the wave front aberrations with small a amount of defocus reintroduced to illustrate that the aberrations in fact follow the annulus of the optic and seem to correspond to a zonal fabrication error.

One primary advantage of at-wavelength interferometry is its ability to characterize the overall EUV wave front produced by both the mirror surface figure and the multilayer coatings. Owing to the fact that, upon a change in wavelength, the aberrations due to multilayers change whereas those due to surface errors do not, multilayer effects can be observed directly via wave front measurements over a range of wavelengths. In this experiment, both transmitted intensity and the wave front phase were measured at several wavelengths. Transmission through the 0.07 NA subaperture of the optic at 13.0, 13.2, 13.4, and 13.6 nm is shown in Fig. 4(a). Transmission through different portions of the aperture reveals a zonal effect that follows the annular full aperture. Within the coating pass band, at 13.2 and 13.4 nm, the transmission is quite uniform, being lower only near the edges of the aperture. The measured transmission along the center of the annulus is peaked at ~13.4 nm wavelength, in agreement with the coating design,[8] but the transmission peak is shifted to ~13.3 nm on the inner edge of the annulus and to ~13.35 nm on the outer edge of the annulus. This indicates

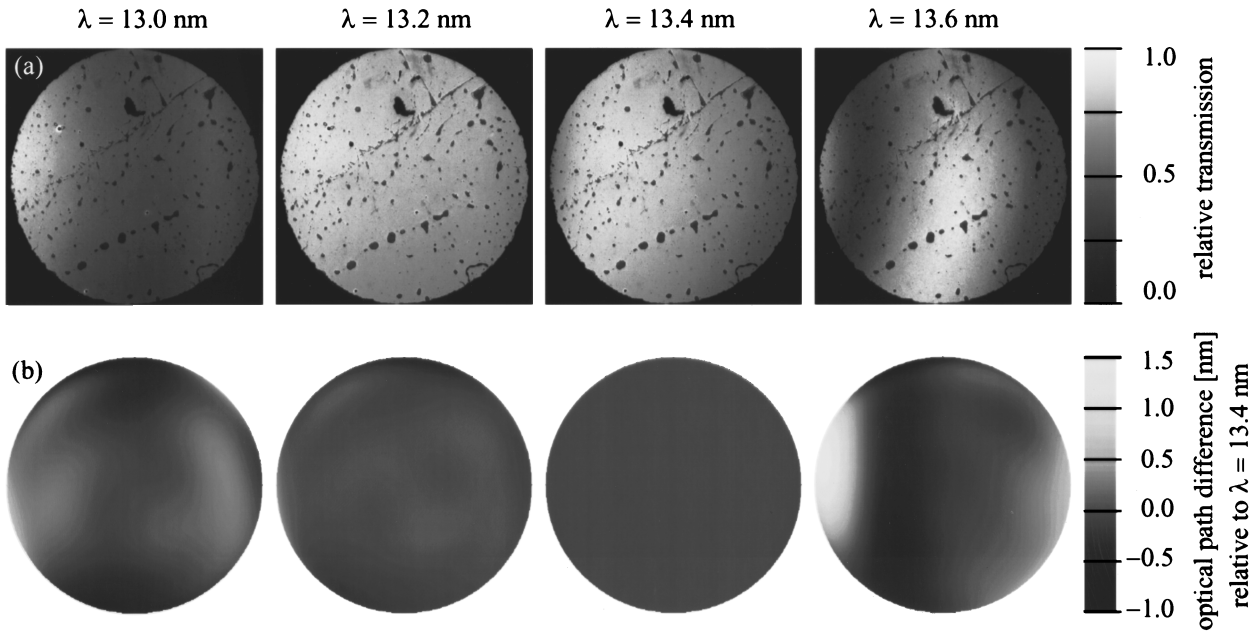

FIG. 4. Measured chromatic aberration produced by multilayer reflective coatings. (a) As the wavelength is changed, transmission through the optic varies. The overall transmission is peaked at 13.4 nm. (b) The measured differences between the aberrations at the indicated wavelengths and the 13.4 nm wavelength demonstrate the presence of multilayer-coating phase effects.

that the multilayer-coating period deviates from its intended value, which is designed to achieve transmission uniformity better than 99% at 13.4 nm. At the edges of the pass band, at 13.0 and 13.6 nm, the transmission is very nonuniform. This behavior is not unexpected, even for perfect multilayers, because the coatings are designed to accommodate a range of incidence angles in a limited spectral band. Outside the design pass band, the differences in incidence angles across the optic are amplified because the coating properties vary rapidly outside the central transmission lobe.

The chromatic phase effects resulting from reflection by multilayer mirrors are illustrated in Fig. 4(b), which shows the difference between the aberrations measured at 13.0, 13.2, 13.4, and 13.6 nm and the aberrations measured at 13.4 nm. Within the coating pass band, the differences in the measured wave fronts are small because the wavelength change results primarily in a constant phase offset that is not measurable by interferometry. At the pass band edges, where nonuniformities in the coating properties are accentuated, the measured phase difference over the aperture is consistent with a radial nonuniformity in the multilayer-coating thickness.

The quality of the interferometry was characterized by repeatability measurements performed on the 0.07 NA subaperture of the Schwarzschild optic. The aberrations were first characterized in a series of measurements performed over several weeks with multiple object–plane input pinholes, several image–plane reference pinholes, and two orthogonal gratings. Following this series of experiments, the other two subapertures of the optic were measured. Subsequently, the 0.07 NA subaperture of the Schwarzschild optic was measured again in a second series of experiments. Successive measurements of each subaperture required removal of the optic from the vacuum chamber, followed by repositioning of the optic and complete realignment of the interferometer. The wave front aberration map and the corresponding Zernike polynomial fit, determined at 13.4 nm wavelength from 23 separate measurements including both series, are shown in Figs. 5(a) and 5(b), respectively. The wave front error of 0.090 ± 0.008 wave (1.21 ± 0.11 nm) rms and 0.531 ± 0.046 wave (7.11 ± 0.61 nm) peak-to-valley, is dominated by astigmatism. The aberrations appear to indicate a zonal fabrication error described earlier. The relatively small aberration magnitude indicates the nearly diffraction-limited quality of the optic. The error bars of the Zernike polynomial coefficients correspond to the rms variation in each term over the 23 measurements. The standard deviations of the 23 measured rms and peak-to-valley wave front aberrations indicate repeatability to within ± 0.008 wave (± 0.11 nm) rms and ± 0.046 wave (± 0.61 nm) peak-to-valley. The absolute accuracy of the measurements is currently under investigation.

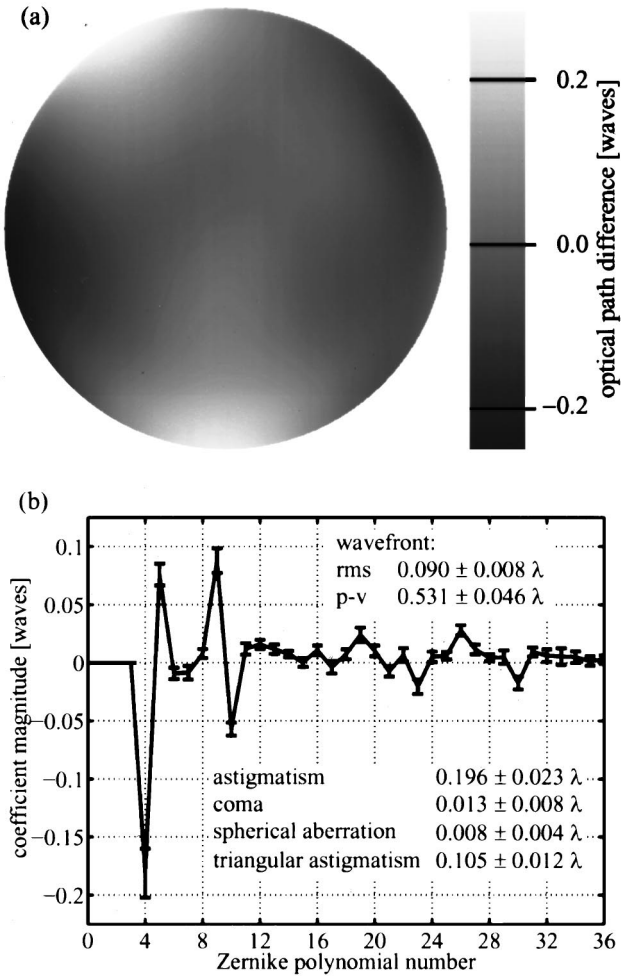

FIG. 5. (a) Wave front aberrations and (b) the Zernike polynomial fit coefficients of the 0.07 NA subaperture of the Schwarzschild optic determined from multiple measurements at 13.4 nm wavelength. The Zernike coefficients correspond to polynomials scaled to have a peak magnitude of 1. The magnitudes of astigmatism (coefficients 4 and 5), coma (6 and 7), spherical aberration (8), and triangular astigmatism (9 and 10) are indicated. The dominant aberration is astigmatism.

IV. VERIFICATION WITH IMAGING EXPERIMENTS

Perhaps the most significant value of interferometric wave front measurements is their ability to predict the imaging performance of optical systems. The interferometry performed here on the 10× Schwarzschild optical system predicts good EUV imaging quality for the 0.07 NA subaperture. The image quality was verified with photoresist exposure experiments performed on the 10×I EUV imaging system[7] at Sandia National Laboratories in Livermore, California. The Sandia exposure tool utilizes imaging optics identical in optical design and housing construction to the Schwarzschild system described here. In this tool, EUV light from a laser-produced plasma is collected by an ellipsoidal condenser and directed via a 45° turning mirror onto a reflective mask/object at near-normal incidence. The mask illumination is of the Köhler type, with a partial coherence factor of approximately 0.5. The image of the mask pattern, produced with the 10× Schwarzschild optic, is recorded on a photoresist-coated wafer.

Prior to the exposure experiments, the interferometry data on the 0.07 NA subaperture were used to calculate the expected image intensities for several test patterns. The images were calculated using the program SPLAT,[15] which simulates

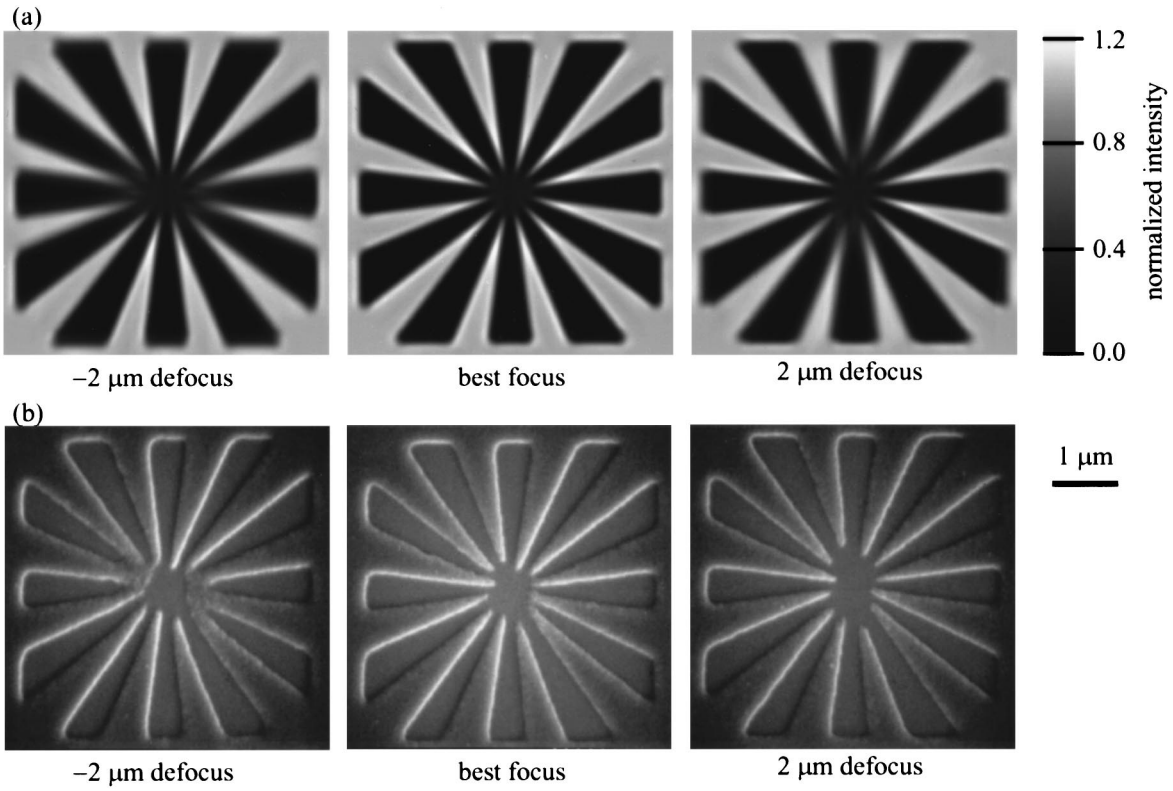

FIG. 6. (a) Image intensities of a bright-field star resolution pattern calculated using the measured aberrations of the Schwarzschild optic. (b) SEM images of the same test pattern recorded experimentally in SAL 601 photoresist show excellent agreement with the calculated prediction.

partially coherent image formation. The calculations were done for a numerical aperture of 0.07, an exposure wavelength of 13.4 nm, an illumination partial coherence factor of 0.5, and the measured aberrations of the Schwarzschild optic. Figure 6(a) shows the calculated image intensity of a bright-field star resolution pattern through focus. The imaging is quite good in all directions at best focus. As is expected of an optic having astigmatism as the dominant aberration, somewhat out of focus, the resolution of the optic improves in one direction but degrades in the orthogonal direction. On the other side of focus, the behavior is similar but with the two directions reversed.

The presence of the aberrations measured in the Schwarzschild system was subsequently verified with photoresist exposure experiments. Negative-tone, chemically amplified, 100-nm-thick, SAL 601 photoresist was used to record images produced by the optic. Figure 6(b) shows scanning electron microscopy (SEM) photographs of the developed photoresist features of the star resolution pattern. The direction of the best resolution changes with defocus, in excellent agreement with the predictions of astigmatic imaging performance. Some of the differences apparent at the center of the patterns are produced by variations in the photoresist exposure dose from image to image.

In summary, the measured aberration magnitude of 0.090 wave rms for the 0.07 NA subaperture predicts near-diffraction-limited optical performance of the Schwarzschild optic. This was observed with the printing of several test patterns, including the star test pattern described here.

V. CONCLUSIONS AND FUTURE WORK

The aberrations of a 10× Schwarzschild optic, designed for EUV lithography experiments, were characterized with a phase-shifting point diffraction interferometer at EUV wavelengths. Measurements of several subregions of the annular aperture indicate the presence of zonal fabrication errors. The 0.07 NA subaperture was found to have relatively small aberrations of 0.090 wave (1.21 nm) rms at 13.4 nm wavelength. The presence of phase aberrations due to multilayer coatings was observed directly with wave front measurements at different wavelengths.

Measurements of the Schwarzschild optic have also served to evaluate the performance of the PS/PDI design and implementation. The measurement repeatability is ± 0.008 wave (± 0.11 nm) rms. Although, determination of the absolute accuracy of the interferometer is still in progress, optical performance predicted from interferometry, evaluated with image calculations that include the effects of the aberrations measured, is consistent with the image quality observed experimentally in the imaging experiments.

ACKNOWLEDGMENTS

The authors would like to thank Senajith B. Rekawa and Charles D. Kemp of the Center for X-Ray Optics at Lawrence Berkeley National Laboratory for mechanical en-

gineering support, and Joshua Cantrell of the University of California at Berkeley for software support. The authors also acknowledge the staff members at the Advanced Light Source at Lawrence Berkeley Laboratory for providing a reliable source of photons. The authors are grateful to Avijit K. Ray-Chaudhuri and Kevin Krenz of Sandia National Laboratories for the opportunity to perform imaging experiments on their exposure tool and for their help with the experiments. The authors also wish to thank Richard H. Livengood of the Intel Corporation for providing access to the focused ion beam tool for pinhole fabrication and Charles H. Fields of the University of California at Berkeley for his help with pinhole fabrication. This research was supported by the Intel Corporation, by the SRC under Contract No. 96-LC-460, by the DARPA Defense Advanced Lithography Program, by the DOE Office of Basic Energy Sciences, and by an Intel Foundation graduate fellowship.

[1]D. T. Attwood, G. Sommargren, R. Beguiristain, K. Nguyen, J. Bokor, N. Ceglio, K. Jackson, M. Koike, and J. Underwood, Appl. Opt. **32**, 7022 (1993).
[2]K. A. Goldberg, R. Beguiristain, J. Bokor, H. Medecki, D. T. Attwood, K. Jackson, E. Tejnil, and G. E. Sommargren, J. Vac. Sci. Technol. B **13**, 2923 (1995).
[3]J. E. Bjorkholm, A. A. MacDowell, O. R. Wood II, Z. Tan, J. B. LaFontaine, and D. M. Tennant, J. Vac. Sci. Technol. B **13**, 2919 (1995).
[4]E. Tejnil, K. A. Goldberg, H. Medecki, R. Beguiristain, J. Bokor, and D. T. Attwood, *OSA Trends in Optics and Photonics Volume on Extreme Ultraviolet Lithography*, edited by G. D. Kubiak and D. R. Kania (Optical Society of America, Washington, DC, 1996), Vol. 4, p. 118.
[5]H. Medecki, E. Tejnil, K. A. Goldberg, and J. Bokor, Opt. Lett. **21**, 1526 (1996).
[6]K. A. Goldberg, E. Tejnil, S. H. Lee, H. Medecki, D. T. Attwood, K. H. Jackson, and J. Bokor, Proc. SPIE **3048**, 264 (1997).
[7]D. A. Tichenor, A. K. Ray-Chaudhuri, G. D. Kubiak, S. J. Haney, K. W. Berger, R. P. Nissen, G. A. Wilkerson, R. H. Stulen, P. H. Paul, R. W. Arling, T. E. Jewell, E. Tejnil, W. C. Sweatt, W. W. Chow, J. E. Bjorkholm, R. R. Freeman, M. D. Himel, A. A. MacDowell, D. M. Tennant, L. A. Fetter, O. R. Wood II, W. K. Waskiewicz, D. L. White, and D. L. Windt, *OSA Proceedings on Extreme Ultraviolet Lithography*, edited by F. Zernike and D. T. Attwood (Optical Society of America, Washington, DC, 1995), Vol. 23, p. 89.
[8]D. L. Windt and W. K. Waskiewicz, J. Vac. Sci. Technol. B **12**, 3826 (1994).
[9]C. Cerjan, in Ref. 7, p. 142.
[10]*Optical Shop Testing*, 2nd ed., edited by D. Malacara (Wiley, New York, 1992), Chap. 14.
[11]K. A. Goldberg (unpublished).
[12]V. N. Mahajan, Appl. Opt. **33**, 8125 (1994).
[13]J. Y. Wang and D. E. Silva, Appl. Opt. **19**, 1510 (1980).
[14]D. J. Fisher, J. T. O'Bryan, R. Lopez, and H. P. Stahl, Appl. Opt. **32**, 4738 (1993).
[15]K. K. Toh and A. R. Neureuther, Proc. SPIE **772**, 202 (1987).